Hindawi Publishing Corporation
EURASIP Journal on Wireless Communications and Networking
Volume 2010, Article ID 753129, 14 pages
doi:10.1155/2010/753129

Research Article

TOA Estimator for UWB Backscattering RFID System with Clutter Suppression Capability

Chi Xu and Choi L. Law

Positioning & Wireless Technology Centre, Nanyang Technological University, 50 Nanyang Drive, Research TechnoPlaza, Level 4, BorderX Block, Singapore 637553

Correspondence should be addressed to Chi Xu, chiandlin@hotmail.com

Received 23 November 2009; Revised 20 April 2010; Accepted 9 May 2010

Academic Editor: Richard Kozick

Time of arrival (TOA) estimation in multipath dense environment for UWB backscattering radio frequency identification (RFID) system is challenging due to the presence of strong clutter. In addition, the backscattering RFID system has peculiar signal transmission and modulation characteristics, which are considerably different from conventional communication and localization systems. The existing TOA estimators proposed for conventional UWB systems are inappropriate for the backscattering RFID system since they lack the required clutter suppression capability and do not account for the peculiar characteristics of backscattering system. In this paper, we derive a nondata-aided (NDA) least square (LS) TOA estimator for UWB backscattering RFID system. We show that the proposed estimator is inherently immune to clutter and is robust in under-sampling operation. The effects of various parameter settings on the TOA estimation accuracy are also studied via simulations.

1. Introduction

Backscattering radio frequency identification (RFID) is a type of RFID technology employing tags that do not generate their own signals but reflect the received signals back to the readers. It is widely used in asset tracking, inventory management, health care monitoring, and other fields [1]. Nowadays many RFID applications such as context-aware healthcare require accurate location information with extended operating range. The conventional backscattering RFID system using continuous wave (CW), however, cannot fulfill this requirement due to its poor distance estimation accuracy and limited operating range. Recently, ultra wideband (UWB) signal emerges as a viable solution for the new generation of backscattering RFID system. UWB is defined by Federal Communications Commission (FCC) as signals having a fractional bandwidth larger than 20% or absolute bandwidth of more than 500 MHz [2]. Such enormous bandwidth brings many advantages such as higher ranging accuracy, lower probability of interception, and more resistance to multipath fading as compared to CW signal [3]. Its capability in achieving accurate range and location estimation has been proven analytically and in experiments [4–7]. UWB signal has been applied to backscattering RFID system with localization functionality in [8, 9]. In [8], the concept of UWB pseudorandom backscattering tag is introduced. The tag receives signal only in certain time interval according to a pseudorandom time hopping sequence, slightly delays it and then reflects it back to the reader. In [9], a UWB backscattering RFID tag that is able to apply various modulation schemes is proposed and its potential operating range/data rate tradeoff in the presence of strong clutter is investigated.

Ranging for UWB backscattering RFID system requires estimation of time of arrival (TOA) of the tag response signal at the reader. However, recovering TOA information in environments with dense scatterers is challenging due to the undesired background clutter caused by scatterers other than RFID tags [10]. Clutter paths arriving earlier than the direct path of the desired tag response signal may cause intolerable false alarm rate whereas those overlapping with the direct path may distort its pulse shape. As a result, the estimation accuracy can be severely degraded.

To clean the received signal contaminated by clutter before applying any TOA estimation algorithm, the empty-room or frame-to-frame techniques used in the radar community may be applied [11]. The empty-room technique subtracts the channel response measured in the absence of the target from any received signal comprising of both target response and clutter. Unfortunately, this technique is sensitive to environment changes since any change renders the previously measured empty-room response inappropriate for further use. For the frame-to-frame technique, each measurement consists of two received signals captured at different timings. The technique subtracts one signal from the other to eliminate the clutter that is assumed to be static in each measurement but may change from measurement to measurement. This technique fails if the target does not move or moves little between received timings of the two signals in the same measurement. Besides the empty-room and frame-to-frame techniques, it is also possible to mitigate clutter by proper selection of the modulation sequence used by the tags. In [9], it is shown that if the tag's modulation sequence for antipodal 2-PAM signaling fulfills certain criteria, by averaging over multiple symbols, the received signal is immune to clutter. The study, however, is carried out in the context of data communication under the assumption that perfect pulse synchronization to the first arriving path is achieved, that is, TOA information is known.

There are many existing TOA estimators proposed for UWB system. The channel estimators derived in [12, 13] are able to estimate the delays of the paths and hence can be implicitly used as TOA estimators. A generalized maximum likelihood (GML) estimator is proposed in [14], which performs the channel estimation in a predefined time interval prior to the largest sample and takes the timing of the first channel tap crossing a preset threshold as TOA. The subspace-based TOA estimators are pursued in [15, 16]. Frequency-domain super-resolution TOA estimation with diversity techniques is studied for indoor localization applications in [17]. The computational complexity of the above estimators is high due to their requirements of either estimation of large number of multipath, or eigen value decomposition of matrices with large dimension. Recent works of TOA estimation focus on the development of low-complexity algorithms. A few suboptimal TOA estimation algorithms with reduced computational complexity are introduced in [18, 19]. The cyclostationarity nature of UWB signal is exploited to develop non-data-aided (NDA) TOA estimators [20, 21]. A novel "timing with dirty template" (TDT) synchronization criterion is established in [22] based on which both data-aided (DA) and NDA estimators are derived. As shown in [23], it is also possible to transform timing estimation into a maximum likelihood (ML) amplitude estimation problem and derive a closed form solution for the frame level timing offset. A few threshold-crossing TOA estimators applicable for energy detection (ED) receiver are developed in [24–26]. In [24], a normalized threshold selection adapted to the strength of the received channel profile is proposed. In [25], a threshold selection method based on Kurtosis value is developed which is proven to be robust to channel condition variation. In [26], the threshold is set as a function of propagation delay and simulation results show that considerable performance improvement can be achieved over conventional methods. A TOA estimator allowing long energy integration duration is derived based on unknown pulse shape and GML criterion [27]. Based on least square (LS) criterion, TOA estimators for UWB system are derived in [28, 29]. To speed up the estimation process, different two-stage estimators are proposed where the first stage estimates a coarse TOA and the second stage refines the result [30, 31]. An excellent literature review of UWB TOA estimation is presented in [32]. All these TOA estimators, however, are derived in the context of conventional UWB system which involves one-way channel propagation and the signal modulations are done at the transmitter. Therefore, the channel response to a single transmitted UWB pulse only contains the information of a single data bit. The UWB backscattering RFID system, however, presents a different propagation scenario. It involves roundtrip channel propagation and the signal modulation is performed at the tag which lies in the middle of the roundtrip channel. If the clock of the backscattering tag does not synchronize with the clock of the reader, such modulation incurs mismatch, that is, the front part of a channel response received at the tag may be modulated by one bit while the tail is modulated by the next data bit. Hence the received signal model of UWB backscattering system is significantly different from that of conventional UWB system. Furthermore, the aforementioned TOA estimators do not include clutter in their signal models during the derivation processes and hence they lack of proven clutter suppression capability. Consequently, those TOA estimators cannot be directly applied to UWB backscattering RFID system.

According to the above discussion, the peculiar transmission and modulation characteristics of UWB backscattering system together with the clutter suppression requirement call for a dedicated treatment of the derivation for TOA estimator. With these requirements in mind, we derive a novel NDA LS TOA estimator for the UWB backscattering RFID system with antipodal 2-PAM based on the tag structure proposed in [9]. The proposed estimator is able to recover the TOA information even when the clocks of readers and tags are asynchronous. By examining the properties of the derived estimator, we find that it has inherent immunity to clutter for arbitrary data sequence which is highly desirable for backscattering RFID system. Unlike the aforementioned empty-room and frame-to-frame techniques, such immunity holds regardless of environment changes and does not matter if the tags move or keep stationary. Simulation results indicate that the estimator is robust in undersampling operation.

The rest of the paper is organized as follows. Section 2 describes the system model and signal model. Section 3 derives the LS estimator whose immunity to clutter is discussed in Section 4. Simulation results are presented in Section 5. Finally, a conclusion is drawn in Section 6.

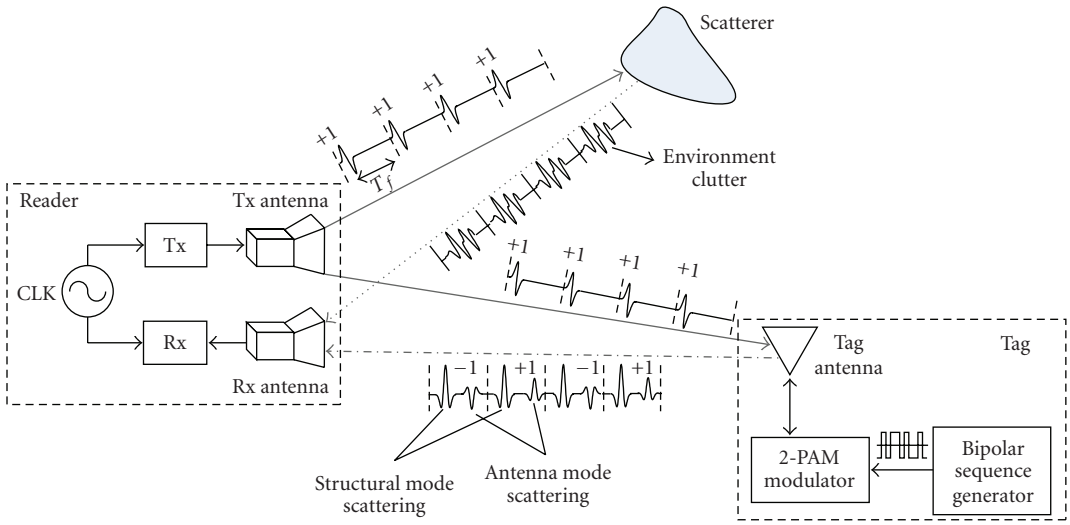

Figure 1: System block diagram.

2. System Model and Signal Model

Here, we derive a NDA LS TOA estimator for the UWB backscattering RFID system with the tag proposed in [9], assuming that the clocks of the reader and tag are asynchronous. Tags under consideration are implemented with antipodal 2-PAM modulators. To initialize the TOA estimation, a reader transmits UWB pulses to a targeted tag and estimates the TOA of the roundtrip channel response. As depicted in Figure 1, the returned roundtrip tag response (including direct transmission and channel echoes) is contaminated by the clutter reflected directly by surrounding scatterers without passing through the tag [10]. With the TOA metric recovered from the received signal, the range between the reader and the tag can be calculated. The range measurements from different readers can be combined to estimate the location of the desired tag. Without loss of generality, we will focus on the TOA estimation between one reader and one tag.

As illustrated in Figure 1, the tag under consideration consists of an antenna, an antipodal 2-PAM modulator and a bipolar sequence generator with output being +1 or −1. The load condition of the tag antenna is determined by the 2-PAM modulator which is controlled by the sequence generator. The 2-PAM modulator retains the polarity of its input signal if +1 is generated by the sequence generator, and it inverts the polarity if −1 is generated. The tag antenna acts like a scatterer and its scattering mechanism can be classified as structural mode and antenna mode [33]. The structural mode scattering is solely determined by the physical properties of the antenna and is independent of the load condition of the antenna. Thus the signal caused by structure mode scattering cannot be modulated by the 2-PAM modulator and hence does not carry any data information in the tag. In contrast, the signal incurred by the antenna mode scattering is received by the antenna and modulated with a bipolar sequence generated by spreading a ranging sequence $\{a_i = \pm 1\}$ with a pseudonoise (PN) code $\{c_j = \pm 1\}$ which has period N_f, that is, $c_{j+N_f} = c_j$, for all j. The PN code $\{c_j\}$ is unique for each tag and is used for multiuser interference suppression or spectrum smoothing. The ranging sequence $\{a_i\}$ is periodic with period N_a. In the following discussion, the tag response refers to the signal caused by the antenna mode scattering while the unmodulated signal caused by the structural mode scattering is treated as part of the clutter.

To initialize the TOA estimation process, the reader repetitively sends UWB pulses starting at timing $t = 0$ with respect to its own clock. Every symbol consists of N_f frames with one pulse per frame. The transmitted signal is given by

$$s(t) = \sum_{i} \sum_{j=0}^{N_f - 1} p_{\text{tx}}\left(t - \left(iN_f + j\right)T_f\right), \tag{1}$$

where $p_{\text{tx}}(t)$ is the transmitted UWB pulse and T_f is the frame duration.

After propagating through the downlink channel (from reader to tag), the transmitted signal with its channel echoes arrives at the tag. Let L_d be the number of paths in the downlink channel. The downlink channel response to $p_{\text{tx}}(t)$ is modeled as

$$h_d(t) = \sum_{l=0}^{L_d - 1} p_d^{(l)}\left(t - \tau_{d\_\text{rel}}^{(l)}\right), \tag{2}$$

where $p_d^{(l)}(t)$ is the pulse of the lth path, $\tau_{d\_\text{rel}}^{(l)} = \tau_d^{(l)} - \tau_d$ is the associated relative path delay, $\tau_d^{(l)}$ and τ_d are the propagation delays of the lth path and the direct path, respectively. $h_d(t)$ has a support region on $[0, T_{\text{ds}}^{(\text{true})}]$ and $T_{\text{ds}}^{(\text{true})}$ is the true maximum delay spread of the one-way channel. Suppose that τ'_{tg} is the processing delay from the tag's receiving antenna to

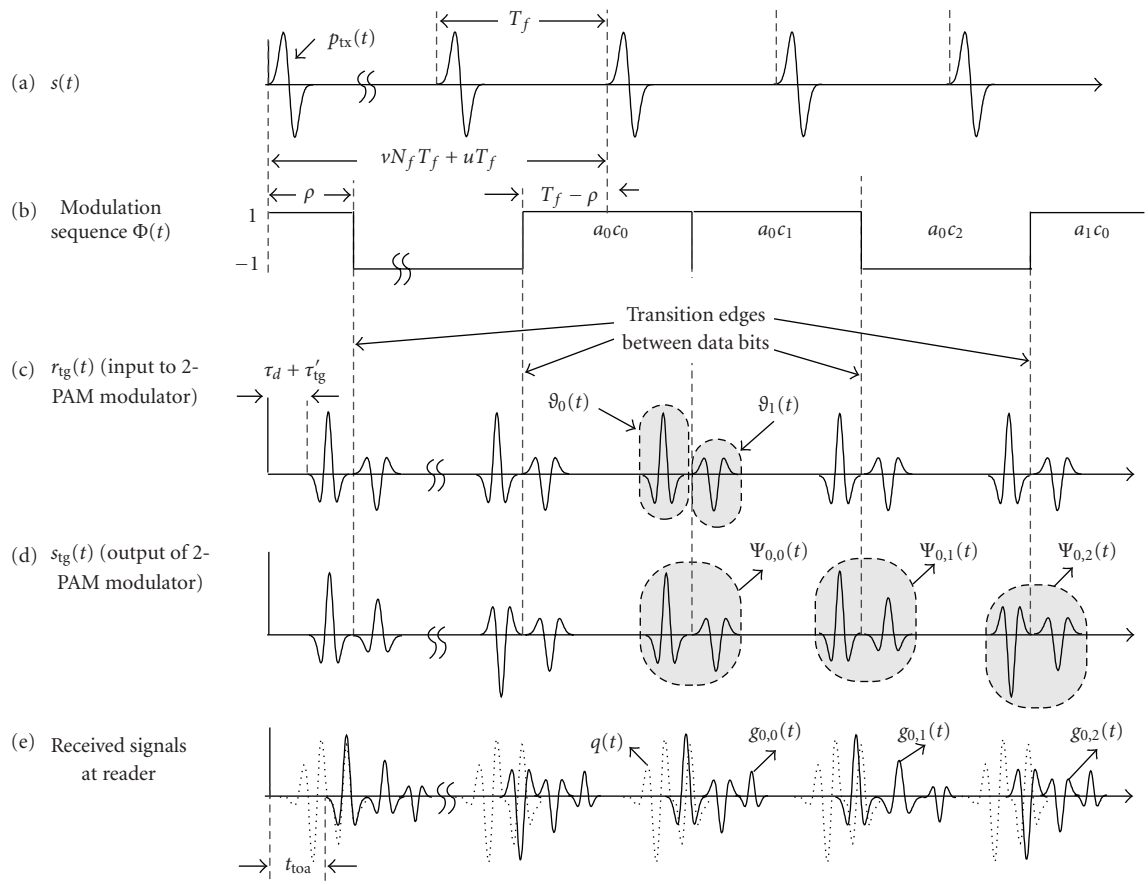

FIGURE 2: Transmited/received signals present at various stages of the RFID system. (For (e), the clutter signal and the tag response are displayed separately).

the modulator. The noise-free signal fed to the modulator of the tag is expressed as

$$r_{tg}(t) = \sum_{i} \sum_{j=0}^{N_f-1} h_d\left(t - \left(iN_f + j\right)T_f - \tau_d - \tau'_{tg}\right). \quad (3)$$

Let $\Omega(t)$ be a rectangular window with unit amplitude in $t \in [0, 1]$ and zero elsewhere. As illustrated in Figure 2(b), the modulator function of the tag is given by

$$\Phi(t) = \sum_{i} \sum_{j=0}^{N_f-1} a_i c_j \Omega\left(\frac{1}{T_f}\left(t - \left(iN_f + vN_f + j + u\right)T_f + \left(T_f - \rho\right)\right)\right), \quad (4)$$

where v and u are integers denoting the ranging symbol offset and PN code offset between the reader and the tag, $\rho \in [0, T_f)$ is the timing offset between the clocks of the reader and the tag. Let $|x|_y$ be the modular operation(x) mod y and $\lfloor \cdot \rfloor$ be the integer floor operation. Equivalently, (4) may be also written as

$$\Phi(t) = \sum_{i} \sum_{j=0}^{N_f-1} \Lambda_{i,j}\left(t - \left(iN_f + vN_f + j + u\right)T_f\right), \quad (5)$$

where $\Lambda_{i,j}(t) = a_i c_j \Omega(t/\rho) + a_{i+\lfloor (j+1)/N_f \rfloor} c_{|j+1|_{N_f}} \Omega((t-\rho)/(T_f - \rho))$ has time support on $[0, T_f]$. The output of the modulator is expressed as

$$s_{tg}(t) = r_{tg}(t)\Phi(t). \quad (6)$$

Substituting (3) and (5) into (6) yields

$$s_{tg}(t) = \sum_{i} \sum_{j=0}^{N_f-1} \Psi_{i,j}\left(t - \left(iN_f + vN_f + j + u\right)T_f - \tau_d - \tau'_{tg}\right), \quad (7)$$

where $\Psi_{i,j}(t) = a_i c_j \vartheta_0(t) + a_{i+\lfloor (j+1)/N_f \rfloor} c_{|j+1|_{N_f}} \vartheta_1(t)$, $\vartheta_0(t) = h_d(t)\Omega((t + \tau_d + \tau'_{tg})/\rho)$ and $\vartheta_1(t) = h_d(t)\Omega((t - \rho + \tau_d + \tau'_{tg})/(T_f - \rho))$. The physical explanations of $\vartheta_0(t)$ and $\vartheta_1(t)$ are given as follows. As shown in Figures 2(b)–2(d), due to the asynchronism between the clocks of the reader and the tag, for $\tau_d + \tau'_{tg} \le \rho \le \tau_d + \tau'_{tg} + T_{ds}^{(true)}$, the channel response $h_d(t)$ may be modulated by two consecutive data bits if the transition edge between the two data bits splits the channel response into two parts. Here $\vartheta_0(t)$ accounts for the front part of the channel response whereas $\vartheta_1(t)$ represents the tail. For $0 \le \rho < \tau_d + \tau'_{tg}$, we have $\vartheta_0(t) = 0$ since the support region of $h_d(t)$ does not overlap with the nonzero region of

$\Omega((t+\tau_d+\tau'_{\text{tg}})/\rho)$. Similarly, for $\tau_d+\tau'_{\text{tg}}+T_{\text{ds}}^{(\text{true})}<\rho<T_f$, we have $\vartheta_1(t)=0$.

Let τ''_{tg} be the delay from the output of the modulator to the transmitting antenna of the tag. The modulated tag response $s_{\text{tg}}(t)$ is delayed by τ''_{tg} seconds and retransmitted back to the reader via the uplink channel (from tag to reader). Assuming that the uplink channel has L_u paths, its responses to $\vartheta_0(t)$ and $\vartheta_1(t)$ are given by

$$\begin{aligned} x(t) &= \sum_{l=0}^{L_u-1} p_{u0}^{(l)}\left(t-\tau_{u0\_\text{rel}}^{(l)}\right), \\ y(t) &= \sum_{l=0}^{L_u-1} p_{u1}^{(l)}\left(t-\tau_{u1\_\text{rel}}^{(l)}\right), \end{aligned} \tag{8}$$

where $p_{u0}^{(l)}$ and $p_{u1}^{(l)}$ are the responses of the lth path to $\vartheta_0(t)$ and $\vartheta_1(t)$, respectively, $\tau_{u0\_\text{rel}}^{(l)}=\tau_{u0}^{(l)}-\tau_u$ and $\tau_{u1\_\text{rel}}^{(l)}=\tau_{u1}^{(l)}-\tau_u$ are the relative propagation delays associated with $p_{u0}^{(l)}$ and $p_{u1}^{(l)}$, τ_u is the propagation delay of the direct path in the uplink channel, and $\tau_{u0}^{(l)}$ and $\tau_{u1}^{(l)}$ are the propagation delays of the lth path. As illustrated in Figure 1, besides the returned tag response, the reader also inevitably receives clutter. The clutter has consistent waveform over different frames since it is not modulated by the tag. The clutter channel response to a single transmitted UWB pulse $p_{\text{tx}}(t)$ is

$$q(t)=\sum_{l=0}^{L_c-1} p_q^{(l)}\left(t-\tau_q^{(l)}\right), \tag{9}$$

where $p_q^{(l)}(t)$ is the response of the lth path in the clutter channel, $\tau_q^{(l)}$ is the propagation delay of that path, and L_c is the number of clutter paths. $q(t)$ has time support on $[\tau_q^{(0)},\tau_q^{(0)}+T_g]$, where T_g is the maximum clutter spread.

Let us define the true TOA t_{toa} as the arrival timing of the returned direct path in response to the pulse transmitted at $t=0$. By this definition, t_{toa} is equal to the roundtrip propagation delay plus the processing delay of the tag, that is, $t_{\text{toa}}=\tau_d+\tau_u+\tau_{\text{tg}}$, where $\tau_{\text{tg}}=\tau'_{\text{tg}}+\tau''_{\text{tg}}$ is the total processing delay of the tag. For ranging applications, τ_{tg} may be known by the reader via precalibration or communications between the tag and the reader so that eventually it can be calibrated out of estimated t_{toa}. Assume that t_{toa} follows a uniform distribution, that is, $t_{\text{toa}}\sim\mathcal{U}(0,T_{\max})$, where $T_{\max}$ is the maximum TOA. After passing through a zonal bandpass filter with bandwidth W, the overall signal received by the reader can be expressed as

$$\begin{aligned} r(t) &= \sum_i \sum_{j=0}^{N_f-1} g_{i,j}\left(t-\left(iN_f+\nu N_f+j+u\right)T_f-t_{\text{toa}}\right) \\ &\quad +\eta(t)+w(t), \end{aligned} \tag{10}$$

where $w(t)$ accounts for thermal noise and multiple access interference, the double-sided power spectral density of $w(t)$ of $N_0/2$, $\eta(t)=\sum_i\sum_{j=0}^{N_f-1} q(t-(iN_f+j)T_f)$ is the overall clutter waveform with $q(t)$ defined in (9), $g_{i,j}(t)=a_ic_jx(t)+a_{i+\lfloor(j+1)/N_f\rfloor}c_{\lfloor j+1\rfloor_{N_f}}y(t)$ is the uplink channel response to $\Psi_{i,j}(t)$ and can also be interpreted as the overall roundtrip tag response to the UWB pulse transmitted at $t=iN_fT_f+jT_f$, $x(t)$ and $y(t)$ have been defined in (8).

In the above derivation, we have assumed that the uplink channel has the same true maximum one-way channel delay spread $T_{\text{ds}}^{(\text{true})}$ as the downlink channel. We further assume that $T_g\le T_f$ and $T_{\max}+2T_{\text{ds}}^{(\text{true})}\le T_f$ so that the interframe interference (IFI) is avoided. As implied by (10), the tag response energy may vary for different frames since the data bits modulating $x(t)$ and $y(t)$ may be different. It is useful to define an averaged symbol energy to noise ratio $\text{SNR}=E_s/N_0$, where E_s is the energy per symbol of the tag response averaged over all possible data bits, that is, $E_s=N_f\mathbb{E}[\int_0^{T_f}g_{i,j}^2(t)dt]=N_f\int_0^{T_f}(x^2(t)+y^2(t))dt$ and $\mathbb{E}[\cdot]$ is the expectation operator. Another parameter of interest is the signal-to-clutter ratio $\text{SCR}=E_s/(N_fE_q)$, where $E_q=\int_0^{T_f}q^2(t)dt$ and N_fE_q is the energy per symbol of the clutter.

3. LS TOA Estimation

In this section, a LS TOA estimator is derived based on T_{ds} which is the presumed maximum delay spread of the one-way channel. Generally, T_{ds} is not equal to its true value $T_{\text{ds}}^{(\text{true})}$. As shown in Section 5, the discrepancy between T_{ds} and $T_{\text{ds}}^{(\text{true})}$ does affect the estimation accuracy and the optimum value of T_{ds} may be determined via simulation.

The received wave form $r(t)$ expressed in (10) is sampled at frequency $f_s=1/\Delta$ with corresponding period $\Delta=T_f/N$, where N is the total number of samples per frame. $r(t)$ is observed over time duration $N_sN_fT_f$ and is sampled at timings $t=mN_fT_f+nT_f+k\Delta$ with $m=0,1,\ldots,N_s-1$, $n=0,1,\ldots,N_f-1$, and $k=0,1,\ldots,N$. Here, N_s is the number of observed symbols and is assumed to be integer multiples of the ranging sequence's period N_a, that is, $N_s=N_aQ$ and Q is an integer. The reason for considering multiple symbols for TOA estimation is to provide processing gain to suppress noise. The channels for both the tag response and clutter are assumed to be static during the sampling duration. The sample vector in the nth frame of the mth symbol interval is denoted as $\mathbf{r}_{m,n}=[r_{m,n}[0],r_{m,n}[1],\ldots,r_{m,n}[N-1]]^T$. Let $M=\lfloor t_{\text{toa}}/\Delta\rfloor$ and $N_{\text{ds}}=\lfloor 2T_{\text{ds}}/\Delta\rfloor$. Let $\mathbf{x}=[x[0],x[1],\ldots,x[N_{\text{ds}}-1]]^T$ and $\mathbf{y}=[y[0],y[1],\ldots,y[N_{\text{ds}}-1]]^T$ be the sample vectors of $x(t)$ and $y(t)$. Define two column vectors $\mathbf{p}_x(M)=[\mathbf{0}_{M\times1}^T,\mathbf{x}^T,\mathbf{0}_{(N-M-N_{\text{ds}})\times1}^T]^T$ and $\mathbf{p}_y(M)=[\mathbf{0}_{M\times1}^T,\mathbf{y}^T,\mathbf{0}_{(N-M-N_{\text{ds}})\times1}^T]^T$, where $\mathbf{0}$ represents a column vector with all elements being zeros. Both $\mathbf{p}_x(M)$ and $\mathbf{p}_y(M)$ contain N elements each. $\mathbf{r}_{m,n}$ may be modeled as

$$\mathbf{r}_{m,n}=\mathbf{g}_{m,n}(u,v,M)+\mathbf{q}+\mathbf{w}_{m,n}, \tag{11}$$

where $\mathbf{q}=[q[0],q[1],\ldots,q[N-1]]^T$ and $\mathbf{w}_{m,n}=[w_{m,n}[0],w_{m,n}[1],\ldots,w_{m,n}[N-1]]^T$ are $N\times1$ column vectors containing samples of clutter and noise, respectively,

$\mathbf{g}_{m,n}(u,v,M)$ is the sample vector of tag response and is given by

$$\mathbf{g}_{m,n}(u,v,M) = C_{m,n}(u,v)\mathbf{p}_x(M) + C_{m,n+1}(u,v)\mathbf{p}_y(M). \quad (12)$$

Here, $C_{m,n}(u,v) = a_{m-v+\lfloor (n-u)/N_f \rfloor} c_{|n-u|_{N_f}}$ and $C_{m,n+1}(u,v) = a_{m-v+\lfloor (n+1-u)/N_f \rfloor} c_{|n+1-u|_{N_f}}$ are data bits modulating the partial tag responses $\mathbf{x}$ and $\mathbf{y}$, respectively.

To proceed, let $\{\widetilde{M}, \tilde{\mathbf{x}}, \tilde{\mathbf{y}}, \tilde{u}, \tilde{v}, \tilde{\mathbf{q}}\}$ be the candidate values of parameters $\{M, \mathbf{x}, \mathbf{y}, u, v, \mathbf{q}\}$ among which M is the parameter of interest whereas the rest are nuisance parameters. $\{\widetilde{M}, \tilde{\mathbf{x}}, \tilde{\mathbf{y}}, \tilde{u}, \tilde{v}, \tilde{\mathbf{q}}\}$ are chosen to minimize the following nonlinear LS function:

$$\Upsilon\left(\widetilde{M}, \tilde{\mathbf{x}}, \tilde{\mathbf{y}}, \tilde{u}, \tilde{v}, \tilde{\mathbf{q}}\right) = \sum_{m=0}^{N_s-1} \sum_{n=0}^{N_f-1} \left\| \mathbf{r}_{m,n} - \tilde{\mathbf{g}}_{m,n}\left(\tilde{u}, \tilde{v}, \widetilde{M}\right) - \tilde{\mathbf{q}} \right\|^2, \quad (13)$$

where the norm operator $\|\mathbf{z}\|$ computes the Euclidean distance of vector $\mathbf{z}$. The search for global minimum of a general multidimensional nonlinear function usually involves numerical searching using the genetic algorithms, grid searchers or other computational intensive algorithms. Fortunately, the nonlinear cost function (13) has some special properties that allow us to first reduce the variables set to be optimized from $\{\widetilde{M}, \tilde{\mathbf{x}}, \tilde{\mathbf{y}}, \tilde{u}, \tilde{v}, \tilde{\mathbf{q}}\}$ to $\{\widetilde{M}, \tilde{u}, \tilde{v}\}$, which drastically reduces the computational complexity. This reduction procedure can lead to the global minimum of the cost function. The simplified cost function with the reduced variable set $\{\widetilde{M}, \tilde{u}, \tilde{v}\}$ is then minimized by searching over all possible discrete values of the variables to reach the global minimum. The details of minimization procedure are given as follows.

The cost function $\Upsilon(\widetilde{M}, \tilde{\mathbf{x}}, \tilde{\mathbf{y}}, \tilde{u}, \tilde{v}, \tilde{\mathbf{q}})$ has two special properties. The first property is that it is a general convex quadratic function of $\tilde{\mathbf{q}}$. By substituting (12) into (13), it can be readily shown that the nonlinear function $\Upsilon(\widetilde{M}, \tilde{\mathbf{x}}, \tilde{\mathbf{y}}, \tilde{u}, \tilde{v}, \tilde{\mathbf{q}})$ can be transformed into the following general convex quadratic form of $\tilde{\mathbf{q}}$ [34, 35]:

$$\begin{aligned}\Upsilon\left(\widetilde{M}, \tilde{\mathbf{x}}, \tilde{\mathbf{y}}, \tilde{u}, \tilde{v}, \tilde{\mathbf{q}}\right) &= \frac{1}{2}\tilde{\mathbf{q}}^T\mathbf{P}_0\tilde{\mathbf{q}} + \boldsymbol{\xi}_0^T\tilde{\mathbf{q}} + \varsigma_0 \\ &= N_sN_f\|\tilde{\mathbf{q}}\|^2 + \boldsymbol{\xi}_0^T\tilde{\mathbf{q}} + \varsigma_0,\end{aligned} \quad (14)$$

where $\mathbf{P}_0 = 2N_sN_f > 0$, $\boldsymbol{\xi}_0 = -2\sum_{m=0}^{N_s-1}\sum_{n=0}^{N_f-1}(\mathbf{r}_{m,n} - \tilde{\mathbf{g}}_{m,n}(\tilde{u}, \tilde{v}, \widetilde{M}))$, $\varsigma_0 = \sum_{m=0}^{N_s-1}\sum_{n=0}^{N_f-1}\|\mathbf{r}_{m,n} - \tilde{\mathbf{g}}_{m,n}(\tilde{u}, \tilde{v}, \widetilde{M})\|^2$.

The second property is that the cost function is twice continuously differentiable with respect to $\tilde{\mathbf{q}}$. This can be readily shown by differentiating (14) twice with respect to $\tilde{\mathbf{q}}$, which yields

$$\frac{\partial^2\Upsilon\left(\widetilde{M}, \tilde{\mathbf{x}}, \tilde{\mathbf{y}}, \tilde{u}, \tilde{v}, \tilde{\mathbf{q}}\right)}{\partial(\tilde{\mathbf{q}})^2} = N_sN_f. \quad (15)$$

The treatments for such special unconstrained convex optimization problem can be found in many books such as [34]. For such special convex function of $\tilde{\mathbf{q}}$, the partial differentiation equation with respect to the variable $\tilde{\mathbf{q}}$ leads to the global minimum of the function. For this reason, we can substitute the solution of partial differential equation $\partial\Upsilon(\widetilde{M}, \tilde{\mathbf{x}}, \tilde{\mathbf{y}}, \tilde{u}, \tilde{v}, \tilde{\mathbf{q}})/\partial\tilde{\mathbf{q}} = 0$ into (13) to eliminate $\tilde{\mathbf{q}}$. Solving $\partial\Upsilon(\widetilde{M}, \tilde{\mathbf{x}}, \tilde{\mathbf{y}}, \tilde{u}, \tilde{v}, \tilde{\mathbf{q}})/\partial\tilde{\mathbf{q}} = 0$ for $\tilde{\mathbf{q}}$ yields the intermediate expression

$$\tilde{\mathbf{q}}' = \boldsymbol{\theta} - \frac{1}{N_sN_f}A_x(\tilde{u}, \tilde{v})\tilde{\mathbf{p}}_x\left(\widetilde{M}\right) - \frac{1}{N_sN_f}A_y(\tilde{u}, \tilde{v})\tilde{\mathbf{p}}_y\left(\widetilde{M}\right), \quad (16)$$

where $\boldsymbol{\theta} = (1/(N_sN_f))\sum_{m=0}^{N_s-1}\sum_{n=0}^{N_f-1}\mathbf{r}_{m,n}$ is an $N \times 1$ vector containing the samples averaged over N_sN_f frames, $\tilde{\mathbf{p}}_x(\widetilde{M}) = [\mathbf{0}^T_{\widetilde{M}\times 1}, \tilde{\mathbf{x}}^T, \mathbf{0}^T_{(N-\widetilde{M}-N_{\mathrm{ds}})\times 1}]^T$, $\tilde{\mathbf{p}}_x(\widetilde{M}) = [\mathbf{0}^T_{\widetilde{M}\times 1}, \tilde{\mathbf{y}}^T, \mathbf{0}^T_{(N-\widetilde{M}-N_{\mathrm{ds}})\times 1}]^T$, $A_x(\tilde{u}, \tilde{v})$ and $A_y(\tilde{u}, \tilde{v})$ are defined as

$$\begin{aligned}A_x(\tilde{u}, \tilde{v}) &= \sum_{m=0}^{N_s-1}\sum_{n=0}^{N_f-1} C_{m,n}(\tilde{u}, \tilde{v}), \\ A_y(\tilde{u}, \tilde{v}) &= \sum_{m=0}^{N_s-1}\sum_{n=0}^{N_f-1} C_{m,n+1}(\tilde{u}, \tilde{v}).\end{aligned} \quad (17)$$

As shown in Appendix A

$$A_x(\tilde{u}, \tilde{v}) = A_y(\tilde{u}, \tilde{v}) = Q\left(\sum_{j=0}^{N_f-1} c_j\right)\left(\sum_{i=0}^{N_a-1} a_i\right) \triangleq A, \quad (18)$$

where A is a constant and is irrelevant to $\{\tilde{u}, \tilde{v}\}$. Using (18), Equation (16) is rewritten as

$$\tilde{\mathbf{q}}' = \boldsymbol{\theta} - \frac{1}{N_sN_f}A\left(\tilde{\mathbf{p}}_x\left(\widetilde{M}\right) + \tilde{\mathbf{p}}_y\left(\widetilde{M}\right)\right). \quad (19)$$

Before proceeding to the next step, let us first define a few terms that will be used in the later discussions

$$\begin{aligned}B_k(\tilde{u}, \tilde{v}) &= \sum_{m=0}^{N_s-1}\sum_{n=0}^{N_f-1} r_{m,n}[k]C_{m,n}(\tilde{u}, \tilde{v}), \\ D_k(\tilde{u}, \tilde{v}) &= \sum_{m=0}^{N_s-1}\sum_{n=0}^{N_f-1} r_{m,n}[k]C_{m,n+1}(\tilde{u}, \tilde{v}),\end{aligned} \quad (20)$$

$$F(\tilde{u}, \tilde{v}) = \sum_{m=0}^{N_s-1}\sum_{n=0}^{N_f-1} C_{m,n}(\tilde{u}, \tilde{v})C_{m,n+1}(\tilde{u}, \tilde{v}). \quad (21)$$

It is shown in Appendix A that $F(\tilde{u}, \tilde{v})$ can be developed as

$$F(\tilde{u}, \tilde{v}) = Q\left(\sum_{i=0}^{N_a-1} a_ia_{i+1}\right)\left(c_{N_f-1}c_0\right) + QN_a\left(\sum_{i=0}^{N_f-2} c_jc_{j+1}\right) \triangleq F, \quad (22)$$

where F is a constant irrelevant to $\tilde{u}$ and $\tilde{v}$.

With equations (19)–(22), by substituting $\tilde{\mathbf{q}} = \tilde{\mathbf{q}}'$ into (13) and dropping the factor $(\sum_m \sum_n \|\mathbf{r}_{m,n}\|^2) - \|\boldsymbol{\theta}\|^2$ which is irrelevant to the decision-making process, we reach

$$\begin{aligned}
&\Upsilon\left(\widetilde{M}, \tilde{\mathbf{x}}, \tilde{\mathbf{y}}, \tilde{u}, \tilde{v}, \tilde{\mathbf{q}}'\right) \\
&\quad = \sum_{m=0}^{N_s-1} \sum_{n=0}^{N_f-1} \Big\| \mathbf{r}_{m,n} - C_{m,n}(\tilde{u}, \tilde{v}) \tilde{\mathbf{p}}_x\left(\widetilde{M}\right) \\
&\qquad\qquad - C_{m,n+1}(\tilde{u}, \tilde{v}) \tilde{\mathbf{p}}_y\left(\widetilde{M}\right) - \tilde{\mathbf{q}}' \Big\|^2 \\
&\quad = \gamma_0 \|\tilde{\mathbf{x}}\|^2 + \gamma_0 \|\tilde{\mathbf{y}}\|^2 - 2\boldsymbol{\beta}_0^T \tilde{\mathbf{x}} - 2\boldsymbol{\beta}_1^T \tilde{\mathbf{y}} + 2\gamma_1 (\tilde{\mathbf{x}})^T \tilde{\mathbf{y}},
\end{aligned} \tag{23}$$

where $\gamma_0 = N_s N_f - A^2/(N_s N_f)$, $\gamma_1 = F - A^2/(N_s N_f)$, $\boldsymbol{\beta}_0 = \boldsymbol{\theta}_B - A\boldsymbol{\theta}_c$, and $\boldsymbol{\beta}_1 = \boldsymbol{\theta}_D - A\boldsymbol{\theta}_c$, $\boldsymbol{\theta}_B, \boldsymbol{\theta}_D$ and $\boldsymbol{\theta}_c$ are $N_{\text{ds}} \times 1$ vectors with their respective kth elements being $\theta_B[k] = B_{k+\widetilde{M}}(\tilde{u}, \tilde{v})$, $\theta_D[k] = D_{k+\widetilde{M}}(\tilde{u}, \tilde{v})$, and $\theta_c[k] = \theta[k + \widetilde{M}]$, for all $0 \le k \le N_{\text{ds}} - 1$. Note that γ_0, γ_1, $\boldsymbol{\beta}_0$, and $\boldsymbol{\beta}_1$ only depend on the observed samples, the ranging and the PN codes.

Similar to the original cost function $\Upsilon(\widetilde{M}, \tilde{\mathbf{x}}, \tilde{\mathbf{y}}, \tilde{u}, \tilde{v}, \tilde{\mathbf{q}})$, the intermediate function $\Upsilon(\widetilde{M}, \tilde{\mathbf{x}}, \tilde{\mathbf{y}}, \tilde{u}, \tilde{v}, \tilde{\mathbf{q}}')$ expressed in (23) also fulfills the two special properties. First, Equation (23) may be transformed into convex quadratic forms of $\tilde{\mathbf{x}}$ and $\tilde{\mathbf{y}}$.

$$\begin{aligned}
\Upsilon\left(\widetilde{M}, \tilde{\mathbf{x}}, \tilde{\mathbf{y}}, \tilde{u}, \tilde{v}, \tilde{\mathbf{q}}'\right) &= \frac{1}{2} \tilde{\mathbf{x}}^T \mathbf{P}_1 \tilde{\mathbf{x}} + \boldsymbol{\xi}_1^T \tilde{\mathbf{x}} + \varsigma_1 \\
&= \gamma_0 \|\tilde{\mathbf{x}}\|^2 + \boldsymbol{\xi}_1^T \tilde{\mathbf{x}} + \varsigma_1, \\
\Upsilon\left(\widetilde{M}, \tilde{\mathbf{x}}, \tilde{\mathbf{y}}, \tilde{u}, \tilde{v}, \tilde{\mathbf{q}}'\right) &= \frac{1}{2} \tilde{\mathbf{y}}^T \mathbf{P}_2 \tilde{\mathbf{y}} + \boldsymbol{\xi}_2^T \tilde{\mathbf{y}} + \varsigma_2 \\
&= \gamma_0 \|\tilde{\mathbf{y}}\|^2 + \boldsymbol{\xi}_2^T \tilde{\mathbf{y}} + \varsigma_2,
\end{aligned} \tag{24}$$

where $\mathbf{P}_1 = 2\gamma_0$, $\boldsymbol{\xi}_1 = 2\gamma_1 \tilde{\mathbf{y}} - 2\boldsymbol{\beta}_0$, $\varsigma_1 = \gamma_0 \tilde{\mathbf{y}}^T \tilde{\mathbf{y}} - 2\boldsymbol{\beta}_1^T \tilde{\mathbf{y}}$, $\mathbf{P}_2 = 2\gamma_0$, $\boldsymbol{\xi}_2 = 2\gamma_1 \tilde{\mathbf{x}} - 2\boldsymbol{\beta}_1$, $\varsigma_2 = \gamma_0 \tilde{\mathbf{x}}^T \tilde{\mathbf{x}} - 2\boldsymbol{\beta}_0^T \tilde{\mathbf{x}}$. Since $A = Q(\sum_{j=0}^{N_f-1} c_j)(\sum_{i=0}^{N_a-1} a_i) < QN_f N_a = N_s N_f$, we have $\gamma_0 = N_s N_f - A^2/(N_s N_f) > 0$. Therefore, $\mathbf{P}_1 > 0$ and $\mathbf{P}_2 > 0$. Second, it can be readily shown that (24) is twice differentiable about $\tilde{\mathbf{x}}$ and $\tilde{\mathbf{y}}$, respectively. According to the previous discussions, we may conclude that the solutions of the two partial differentiation equations $\partial\Upsilon(\widetilde{M}, \tilde{\mathbf{x}}, \tilde{\mathbf{y}}, \tilde{u}, \tilde{v}, \tilde{\mathbf{q}}')/\partial\tilde{\mathbf{x}} = 0$ and $\partial\Upsilon(\widetilde{M}, \tilde{\mathbf{x}}, \tilde{\mathbf{y}}, \tilde{u}, \tilde{v}, \tilde{\mathbf{q}}')/\partial\tilde{\mathbf{y}} = 0$ lead to the global minimum of $\Upsilon(\widetilde{M}, \tilde{\mathbf{x}}, \tilde{\mathbf{y}}, \tilde{u}, \tilde{v}, \tilde{\mathbf{q}}')$. Solving the two differentiation equations for $\tilde{\mathbf{x}}$ and $\tilde{\mathbf{y}}$ gives

$$\begin{aligned}
\gamma_0 \tilde{\mathbf{x}} + \gamma_1 \tilde{\mathbf{y}} &= \boldsymbol{\beta}_0, \\
\gamma_1 \tilde{\mathbf{x}} + \gamma_0 \tilde{\mathbf{y}} &= \boldsymbol{\beta}_1.
\end{aligned} \tag{25}$$

Solving (25) gives the following intermediate expressions for tag response:

$$\begin{aligned}
\tilde{\mathbf{x}}' &= \frac{\gamma_1 \boldsymbol{\beta}_1 - \gamma_0 \boldsymbol{\beta}_0}{\gamma_1^2 - \gamma_0^2}, \\
\tilde{\mathbf{y}}' &= \frac{\gamma_1 \boldsymbol{\beta}_0 - \gamma_0 \boldsymbol{\beta}_1}{\gamma_1^2 - \gamma_0^2}.
\end{aligned} \tag{26}$$

With (26), substituting $\tilde{\mathbf{x}} = \tilde{\mathbf{x}}'$ and $\tilde{\mathbf{y}} = \tilde{\mathbf{y}}'$ into (23) and simplifying, we have the following expression for $\Upsilon(\widetilde{M}, \tilde{\mathbf{x}}', \tilde{\mathbf{y}}', \tilde{u}, \tilde{v}, \tilde{\mathbf{q}}')$ depending only on $\{\widetilde{M}, \tilde{u}, \tilde{v}\}$:

$$\Upsilon\left(\widetilde{M}, \tilde{\mathbf{x}}', \tilde{\mathbf{y}}', \tilde{u}, \tilde{v}, \tilde{\mathbf{q}}'\right) = \frac{\gamma_0\left(\left\|\boldsymbol{\beta}_0\right\|^2 + \left\|\boldsymbol{\beta}_1\right\|^2\right) - 2\gamma_1 \boldsymbol{\beta}_1^T \boldsymbol{\beta}_0}{\gamma_1^2 - \gamma_0^2}. \tag{27}$$

Note that (27) is invalid when $\gamma_1^2 - \gamma_0^2 = 0$. To cover this exceptional situation, the following analysis is carried out. The equation $\gamma_1^2 - \gamma_0^2 = 0$ can be factorized as

$$\gamma_1{}^2 - \gamma_0^2 = \left(F - N_s N_f\right)\left(F + N_s N_f - 2A^2/N_s N_f\right) = 0, \tag{28}$$

which leads to

$$F - N_s N_f = 0, \tag{29}$$

$$F + N_s N_f - 2A^2/N_s N_f = 0. \tag{30}$$

In Appendix B, we show that at least one of (29) and (30) holds when the conditions $C_{m,n}(\tilde{u}, \tilde{v}) = C_{m,n+1}(\tilde{u}, \tilde{v})$, for all m, n or $C_{m,n}(\tilde{u}, \tilde{v}) + C_{m,n+1}(\tilde{u}, \tilde{v}) = 0$, for all m, n is met. Next, we will give some intuition for these two conditions. The condition $C_{m,n}(\tilde{u}, \tilde{v}) = C_{m,n+1}(\tilde{u}, \tilde{v})$, for all m, n is met when every bit in the sequence $\{C_{m,n}(\tilde{u}, \tilde{v})\}$ has the same polarity, that is, $C_{m,n}(\tilde{u}, \tilde{v}) = +1$, for all m, n or $C_{m,n}(\tilde{u}, \tilde{v}) = -1$, for all m, n. In this case the tag response will retain polarity over different frames, appearing as "unmodulated" signal like clutter. Therefore, there is no way the tag response can be distinguished from the clutter, which is undesired. In the following discussion, we assume that such undesired sequence is deliberately discarded in the system design so that $F \neq N_s N_f$ applies. The second condition $C_{m,n}(\tilde{u}, \tilde{v}) + C_{m,n+1}(\tilde{u}, \tilde{v}) = 0$, for all m, n is fulfilled when $\{C_{m,n}(\tilde{u}, \tilde{v})\}$ consists of alternative $+1$ and -1, that is, it is a sequence of $+1, -1, +1, -1, \ldots$. With such sequence, we have $A = 0$, $F = -N_s N_f$ and $B_k(\tilde{u}, \tilde{v}) = -D_k(\tilde{u}, \tilde{v})$. Together with (23), it is straightforward to show that

$$\Upsilon\left(\widetilde{M}, \tilde{\mathbf{x}}, \tilde{\mathbf{y}}, \tilde{u}, \tilde{v}, \tilde{\mathbf{q}}'\right) = N_s N_f \|\tilde{\mathbf{x}} - \tilde{\mathbf{y}}\|^2 - 2\boldsymbol{\theta}_B^T (\tilde{\mathbf{x}} - \tilde{\mathbf{y}}). \tag{31}$$

Solving (25) gives

$$\tilde{\mathbf{x}}' - \tilde{\mathbf{y}}' = \frac{1}{N_s N_f} \boldsymbol{\theta}_B. \tag{32}$$

With (32), substituting $\tilde{\mathbf{x}} - \tilde{\mathbf{y}} = \tilde{\mathbf{x}}' - \tilde{\mathbf{y}}'$ into (31) yields

$$\Upsilon\left(\widetilde{M}, \tilde{\mathbf{x}}', \tilde{\mathbf{y}}', \tilde{u}, \tilde{v}, \tilde{\mathbf{q}}'\right) = -\frac{1}{N_s N_f} \|\boldsymbol{\theta}_B\|^2. \tag{33}$$

According to the above discussion, we can conclude our final estimator: for $\{\tilde{u}, \tilde{v}\}$ leading to $\gamma_1^2 = \gamma_0^2$, the decision function $\Upsilon(\widetilde{M}, \tilde{\mathbf{x}}', \tilde{\mathbf{y}}', \tilde{u}, \tilde{v}, \tilde{\mathbf{q}}')$ is directly computed based on (33); else $\Upsilon(\widetilde{M}, \tilde{\mathbf{x}}', \tilde{\mathbf{y}}', \tilde{u}, \tilde{v}, \tilde{\mathbf{q}}')$ is computed using (27). Subsequently, the candidate values $\{\widetilde{M}, \tilde{u}, \tilde{v}\}$ minimizing the value of the decision function $\Upsilon(\widetilde{M}, \tilde{\mathbf{x}}', \tilde{\mathbf{y}}', \tilde{u}, \tilde{v}, \tilde{\mathbf{q}}')$ is adopted as final estimates

$$\left\{\widehat{M}, \hat{u}, \hat{v}\right\} = \arg\min_{\widetilde{M}, \tilde{u}, \tilde{v}} \left[\Upsilon\left(\widetilde{M}, \tilde{\mathbf{x}}', \tilde{\mathbf{y}}', \tilde{u}, \tilde{v}, \tilde{\mathbf{q}}'\right)\right], \tag{34}$$

where $\{\widehat{M}, \hat{u}, \hat{v}\}$ are the final estimates of $\{M, u, v\}$. And the TOA is estimated as

$$\hat{t}_{\text{toa}} = \Delta\widehat{M}. \tag{35}$$

Equation (34) indicates that the final solution involves a minimum search procedure over a three-dimensional space span by variables $\{\widetilde{M}, \tilde{u}, \tilde{v}\}$. The complexity of this searching procedure is proportional to the number of possible discrete values of $\widetilde{M}$, $\tilde{u}$, and $\tilde{v}$, that is, proportional to the maximum number of samples prior to the TOA sample $\lfloor f_s T_{\max} \rfloor$, the number of symbols N_s, and the number of frames per symbol N_f. Reducing f_s or N_s can lower the computational complexity. As a tradeoff, the TOA estimation accuracy will decrease accordingly. However, the simulation results in Section 5 will reveal that the TOA performance is very robust to the reduction in f_s and is reduced by only about 3 dB for halving N_s. Reducing N_f also reduces the computational complexity which causes insignificant variation of TOA estimation as shown in the simulation results in Section 5. Therefore, our scheme does not require large N_f and N_f should be minimized for TOA estimation during system design phase. This minimum value of N_f should be determined by other aspects of system design such as spectrum smoothing or the number of users in the system, which is out of the scope of this paper. Hence, by carefully setting f_s, N_s, and N_f, satisfactory performance can be achieved with reasonable complexity.

4. Immunity of the Estimator to Clutter

Any TOA estimator for UWB backscattering RFID system should posses clutter suppression capability, especially in an environment with dense scatterers. In [9], for data communication applications, clutter is suppressed by choosing a data sequence with zero mean (or quasi-zero mean). Intuitively we would have expected that similar sequence selection should also be imposed to ensure that the estimator derived in Section 3 is immune to clutter. However, we are going to show that the derived estimator is indeed inherently immune to clutter for arbitrary data sequence.

Note that the final decision function $\Upsilon(\widetilde{M}, \tilde{\mathbf{x}}', \tilde{\mathbf{y}}', \tilde{u}, \tilde{v}, \tilde{\mathbf{q}}')$ is computed based on sample set $\{r_{m,n}[k]\}$ which is a function of the true tag response $\{x[k], y[k]\}$, clutter $\{q[k]\}$, and noise $\{w_{m,n}[k]\}$. Recall that $\Upsilon(\widetilde{M}, \tilde{\mathbf{x}}', \tilde{\mathbf{y}}', \tilde{u}, \tilde{v}, \tilde{\mathbf{q}}')$ is computed using (27) for $\gamma_1^2 \neq \gamma_0^2$ and using (33) for $\gamma_1^2 = \gamma_0^2$. To explicitly reveal the possible effects of the clutter term $\{q[k]\}$ on $\Upsilon(\widetilde{M}, \tilde{\mathbf{x}}', \tilde{\mathbf{y}}', \tilde{u}, \tilde{v}, \tilde{\mathbf{q}}')$ given in (27), the signal model $r_{m,n}[k]$ given in (11) is substituted into (27), which yields

$$\begin{aligned}
&\Upsilon\left(\widetilde{M}, \tilde{\mathbf{x}}', \tilde{\mathbf{y}}', \tilde{u}, \tilde{v}, \tilde{\mathbf{q}}'\right) \\
&\quad = \frac{\gamma_0 \left\| (\gamma_0 - \gamma_1)\left(\mathbf{z}_x - \mathbf{z}_y\right) + \mathbf{f}_{w0} - \mathbf{f}_{w1} \right\|^2}{\gamma_1^2 - \gamma_0^2} \\
&\qquad + \frac{2\left(\gamma_0 \mathbf{z}_x + \gamma_1 \mathbf{z}_y + \mathbf{f}_{w0}\right)^T \left(\gamma_1 \mathbf{z}_x + \gamma_0 \mathbf{z}_y + \mathbf{f}_{w1}\right)}{(\gamma_0 + \gamma_1)},
\end{aligned} \tag{36}$$

where $\mathbf{z}_x$ and $\mathbf{z}_y$, $\mathbf{f}_{w0}$ and $\mathbf{f}_{w1}$ are $(N_{\text{ds}} - 1) \times 1$ vectors with their kth element given by $z_x[k] = p_x[k + \widetilde{M}]$, $z_y[k] = p_y[k + \widetilde{M}]$,

$$\begin{aligned}
f_{w0}[k] &= \sum_{m=0}^{N_s-1} \sum_{n=0}^{N_f-1} w_{m,n}\left[k + \widetilde{M}\right]\left(C_{m,n}(\tilde{u}, \tilde{v}) - \frac{A}{N_s N_f}\right), \\
f_{w1}[k] &= \sum_{m=0}^{N_s-1} \sum_{n=0}^{N_f-1} w_{m,n}\left[k + \widetilde{M}\right]\left(C_{m,n+1}(\tilde{u}, \tilde{v}) - \frac{A}{N_s N_f}\right).
\end{aligned} \tag{37}$$

By observing (36) and (37), it is found that all the terms with symbolic term $\{q[k]\}$ have been completely cancelled out during the derivation process, leaving no clutter term in the final expression. This finding suggests that clutter does not have any effect on the value of decision function. Therefore, the decision function (27) is immune to the clutter.

Next, to prove that (33) is immune to the clutter, we recall that (33) is used for $C_{m,n}(\tilde{u}, \tilde{v}) + C_{m,n+1}(\tilde{u}, \tilde{v}) = 0$, for all m, n which leads to equations $A = 0$, $F = -N_s N_f$ and $B_k(\tilde{u}, \tilde{v}) = -D_k(\tilde{u}, \tilde{v})$ as discussed in Section 3. With these equations and (11), (33) is written as

$$\Upsilon\left(\widetilde{M}, \tilde{\mathbf{x}}', \tilde{\mathbf{y}}', \tilde{u}, \tilde{v}, \tilde{\mathbf{q}}'\right) = -\frac{1}{N_s N_f}\left\| N_s N_f \left(\mathbf{z}_x - \mathbf{z}_y\right) + \mathbf{f}_{w2} \right\|^2, \tag{38}$$

where $\mathbf{f}_{w2}$ is a $(N_{\text{ds}} - 1) \times 1$ vector with its kth element given by

$$f_{w2}[k] = \sum_{m=0}^{N_s-1} \sum_{n=0}^{N_f-1} w_{m,n}\left[k + \widetilde{M}\right] C_{m,n}(\tilde{u}, \tilde{v}). \tag{39}$$

The absence of clutter term $\{q[k]\}$ in (38) implies that the decision function (33) is also irrelevant to the clutter.

Consequently, based on the above discussions, it can be concluded that the proposed estimator is immune to the clutter. This conclusion is also supported by the simulation results presented in the next section.

5. Simulation Results

For the tag response, the impulse responses of both downlink and uplink channels are generated from the channel models CM1 for residential LOS environment and CM2 for residential NLOS environment as described in IEEE802.15.4a standard [36]. The lengths of the generated one-way channel impulse responses are truncated beyond 60 ns, that is, $T_{\text{ds}}^{(\text{true})} = 60$ ns which is the same setting as used in [28] and can capture 99.97% and 90.87% of total channel energy of CM1 and CM2, respectively. Since no UWB channel model for clutter has been reported in the literature, the impulse response of the clutter channel used in simulations is generated as follows. Let $h_{\text{IR\_}q}(t)$ be the impulse response of the clutter. $h_{\text{IR\_}q}(t)$ is generated by

$$h_{\text{IR\_}q}(t) = h_{\text{IR}}(t) \otimes h_{\text{IR}}(t) \otimes \delta\left(t - t_q\right), \tag{40}$$

Table 1: Summary of Adopted Symbols for Simulation.

Symbol	Definition	Value
$T_{\text{ds}}^{(\text{true})}$	True maximum length of one-way tag response	60 ns
T_g	Maximum length of roundtrip clutter response	150 ns
$T_{\max}$	Maximum roundtrip propagation delay of tag response and clutter response	40 ns
N_a	Code period of ranging sequence $\{a_i\}$	8
N_{ch}	The total number of channel realizations	1000
W	Signal bandwidth	4 GHz
τ_{tg}	Tag processing delay	0

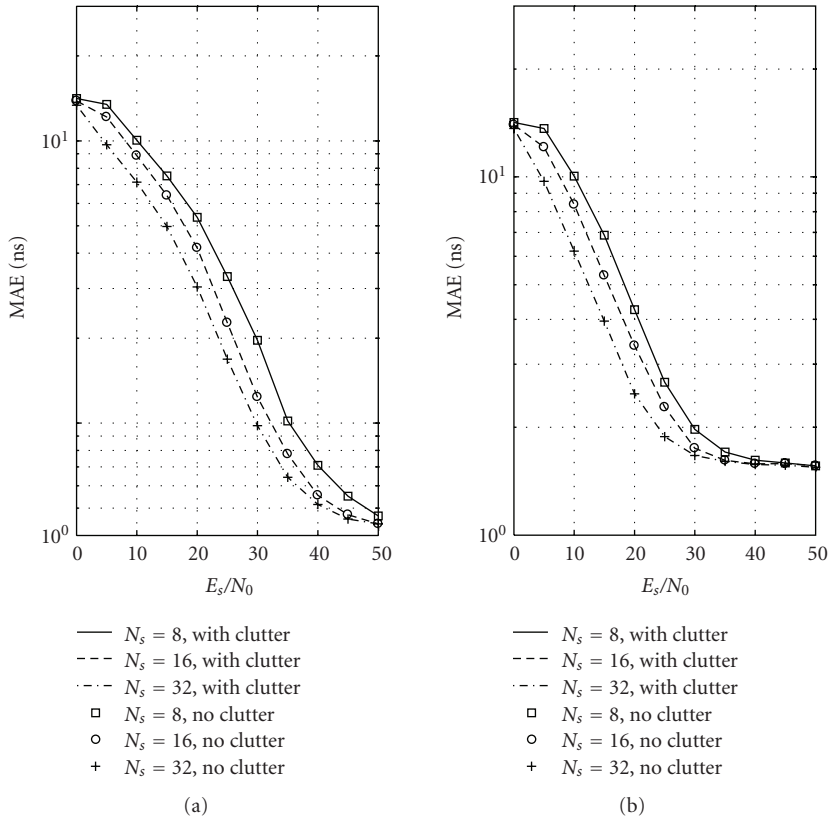

Figure 3: Performance comparison of the estimator under the scenarios with and without clutter for different number of sampled symbols in CM1 (a) and CM2 (b) with $T_{\text{ds}} = 45$ ns, $f_s = 8$ GHz, $N_f = 4$, and SCR $= -30$ dB.

where $\otimes$ is the convolution operator, and $h_{\text{IR}}(t)$ is a one-way channel impulse response generated independently and randomly from the CM1 and CM2 channel models used for the tag response generation, $\delta(t)$ is a Dirac delta function and t_q is the propagation delay of the first path in the clutter. Assume that t_q follows a uniform distribution, that is, $t_q \sim \mathcal{U}(0, T_{\max})$. The length of clutter responses are truncated beyond $T_g = 150$ ns which is slightly longer than the true maximum roundtrip delay spread of tag responses $2T_{\text{ds}}^{(\text{true})} = 120$ ns.

The transmitted UWB pulse is shaped as the second derivative of Gaussian pulse with width of 1 ns. Without loss of generality, we set the tag processing delay to zero in the simulation, that is, $\tau_{\text{tg}} = 0$ ns. The rest of system settings are $W = 4$ GHz, $T_{\max} = 40$ ns, $T_f = 200$ ns, $N_a = 8$. For each channel realization, the sequence $\{a_i\}$ and $\{c_j\}$ are randomly generated. The TOA estimation error for the κth channel realization is $\varepsilon_\kappa = \hat{t}_{\text{toa}} - t_{\text{toa}}$ and the mean absolute error (MAE) defined by $\text{MAE} = (1/N_{\text{ch}}) \sum_{\kappa=0}^{N_{\text{ch}}-1} |\varepsilon_\kappa|$ is used as performance criterion where N_{ch} is the total number of channel realizations and is set to 1000 in the simulation. The symbols adopted in the simulations are summarized in Table 1.

Figure 3 compares the MAEs of the LS TOA estimator in the scenarios with clutter and without clutter. The system settings are $f_s = 8$ GHz, $N_f = 4$, and $T_{\text{ds}} = 45$ ns. The SCR is set to -30 dB representing the extreme environment where the clutter overwhelms the signal. It is found that regardless of the variation in channel condition and the number of observed symbols, the estimator is immune to the clutter.

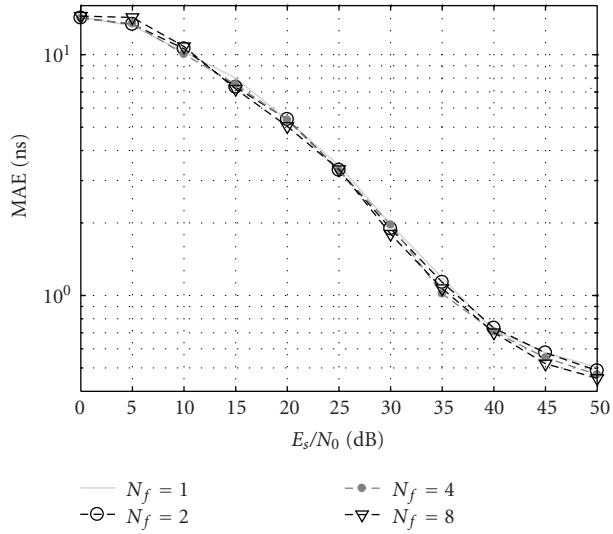

Figure 4: Performance comparison with different N_f in CM1 with $T_{ds} = 45$ ns, $f_s = 8$ GHz, and SCR $= -30$ dB.

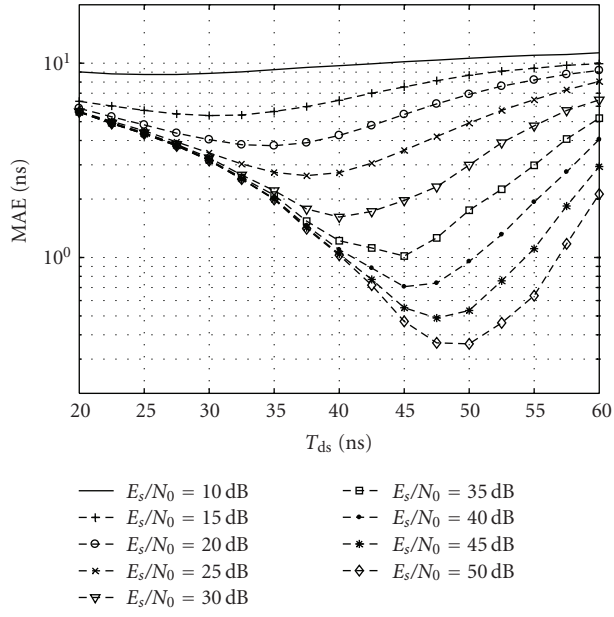

Figure 5: MAE versus channel delay spread setting for different SNR in CM1 with $N_s = 8$, $N_f = 4$, and $f_s = 8$ GHz.

Figure 3 indicates that the MAE of CM1 is generally lower than that of CM2 especially in the high SNR region. The reason is that the direct path is statistically stronger in CM1 than in CM2 due to the obstacles in CM2 environment that may severely attenuate the direct path. It can also be observed that using more symbols improves the performance of the estimator. In both CM1 and CM2, for a large range of SNR, doubling the number of sampled symbols results in 3 dB less SNR to achieve a given MAE.

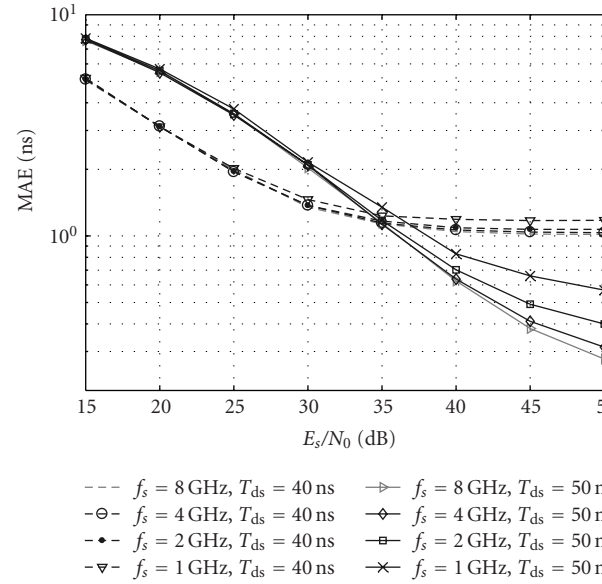

Figure 6: Effect of sampling frequency on MAE in CM1 with N_s =16 and $N_f = 4$ for $T_{ds} = 40$ ns (dash line) and $T_{ds} = 50$ ns (solid line).

Figure 4 investigates the effects of the number of frames per symbol N_f on the performance with $T_{ds} = 45$ ns, $f_s = 8$ GHz, and SCR $= -30$ dB. As N_f increases from 1 to 8, the variation of MAE is insignificant which suggests that the impact of N_f on the estimation accuracy is trivial. Moreover, according to (34), the computational complexity of the proposed estimator increases as N_f increases. Hence N_f should be minimized for TOA estimation purpose during system design phase.

Setting of the presumed maximum one-way channel delay spread T_{ds} is closely related to the performance of TOA estimation since it directly determines N_{ds} which is included in the discrete signal model used to derive LS estimator. Figure 5 presents the results of MAE versus T_{ds} for different SNR values in CM1 channels which have RMS delay spread of around 17 ns. The system settings are $N_s = 16$ and $N_f = 4$. There is an optimal setting of T_{ds} for every SNR curve. This optimal setting ranges from 25 ns to 50 ns as SNR varies from 10 to 50 dB and it increases as SNR increases. The MAE is much more sensitive to the setting of T_{ds} for signal with high SNR.

Figure 6 shows the MAE of the estimator operating with various sampling rates for the presumed delay spread of $T_{ds} = 40$ ns and 50 ns. The system settings are $N_s = 8$ and $N_f = 4$. $f_s = 8$ GHz is the Nyquist rate while $f_s = 1$ GHz is the sampling rate equal to the inverse of pulse width. As expected, the MAE increases as the sampling rate decreases. The MAE performance difference between different sampling rates is reduced as SNR decreases. At moderate SNR level, for instance, SNR $= 35$ dB, the MAE difference between $f_s = 8$ GHz and $f_s = 1$ GHz is only 0.1 ns for $T_{ds} = 40$ ns and 0.2 ns for $T_{ds} = 50$ ns. Therefore, we may conclude that the estimator is robust over undersampling operation.

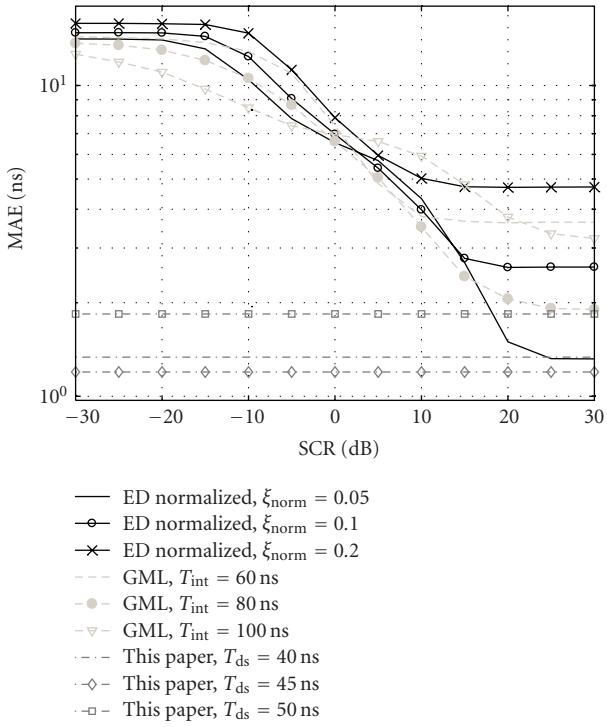

Figure 7: Performance comparison of different TOA estimators in CM1: (1) ED estimator with normalized threshold (solid line); (2) estimator derived based on GML criterion (dash line); (3) the estimator proposed in this paper (dash-dot line). The settings are $E_s/N_0 = 35$ dB, $N_s = 8$, $N_f = 4$, $\Delta = 1$ ns, $T_{\text{GML}} = 1$ ns, and $T_{\text{ED}} = 1$ns, $T_{\text{sb}} = 40$ ns.

In Figure 7, we compare the performance of the estimator proposed in this paper with two estimators proposed in [24, 27]. The two estimations are described as follows. The TOA estimator developed in [24] passes the received waveform to a square-law device, integrates the output successively with time interval T_{ED} to obtain energy samples and then searches the direct path sample within a time period prior to the strongest sample. Note that T_{ED} is the time resolution for this estimator. The search back window is denoted as T_{sb} and the number of energy samples within the windows are $N_{\text{sb}} = \lfloor T_{\text{sb}}/T_{\text{ED}} \rfloor$. The first sample crossing a predefined normalized threshold γ_{norm} is detected as the direct path sample. The energy samples for this estimator can be expressed as

$$z_{\text{ED}}[k] = \sum_{m=0}^{N_s-1} \sum_{n=0}^{N_f-1} \int_{t=mN_fT_f+nT_f+kT_{\text{ED}}}^{t=mN_fT_f+nT_f+(k+1)T_{\text{ED}}} |r(t)|^2 dt, \quad k = 0, 1, \ldots, \left\lfloor \frac{T_f}{T_{\text{ED}}} \right\rfloor - 1. \tag{41}$$

The normalized threshold γ_{norm} is defined by

$$\gamma_{\text{norm}} = \min[z_{\text{ED}}[k]] + \gamma_{\text{norm}}(\max[z_{\text{ED}}[k]] - \min[z_{\text{ED}}[k]]), \tag{42}$$

where $\min[z_{\text{ED}}[k]]$ and $\max[z_{\text{ED}}[k]]$ are minimum and maximum samples among $\{z_{\text{ED}}[k]\}$. The TOA is estimated as

$$\hat{t}_{\text{toa}} = T_{\text{ED}}(\min[k \mid z_{\text{ED}}[k] > \gamma_{\text{norm}}] - 0.5 + (k_{\max} - N_{\text{sb}} - 1)), \quad \forall k - N_{\text{sb}} \le k \le k_{\max}, \tag{43}$$

where $k_{\max} = \arg\max_k[z_{\text{ED}}[k]]$. This estimator is referred to as ED estimator with normalized threshold hereafter.

The estimator presented in [27] is derived based on GML criterion with the assumption that the shape of the received waveform is unknown. The estimator performs energy integrations successively with long time duration T_{int} comparable to the delay spread of propagation channel. Unlike the estimator in [24], the time intervals of the integrations are allowed to overlap with each other if multiple integrators are implemented in parallel. The starting timings of two adjacent integrations are separated by a fixed delay T_{GML} which determines the time resolution. The samples are

$$z_{\text{GML}}[k] = \sum_{m=0}^{N_s-1} \sum_{n=0}^{N_f-1} \int_{t=mN_fT_f+nT_f+kT_{\text{GML}}}^{t=mN_fT_f+nT_f+kT_{\text{GML}}+T_{\text{int}}} |r(t)|^2 dt, \quad k = 0, 1, \ldots, \left\lfloor \frac{T_f}{T_{\text{GML}}} \right\rfloor - 1. \tag{44}$$

The arrival timing of the maximum sample is taken as TOA

$$\hat{t}_{\text{toa}} = T_{\text{GML}}\left(\arg\max_k[z_{\text{GML}}[k]] - 0.5\right), \quad \forall 0 \le k \le \left\lfloor \frac{T_{\max}}{T_{\text{GML}}} \right\rfloor. \tag{45}$$

Among the two estimators, the ED estimator with normalized threshold is more robust to the channel and noise variation since its adaptive threshold setting while the estimator derived based on GML criterion can potentially achieve higher resolution in practical system since it decouples the time resolution from the length of integration interval and the short interval is difficult to be implemented due to receiver hardware limitation [27].

To perform a fair comparison, we set $T_{\text{ED}} = 1$ ns, $T_{\text{GML}} = 1$ ns, and $\Delta = 1/f_s = 1$ ns so that the time resolution of the three estimators, that is, the ED estimator with normalized threshold, the GML estimator, and the estimator presented in this paper, are the same. The rest of parameter settings are SNR $= E_s/N_0 = 35$ dB, $N_s = 8$, and $N_f = 8$. Figure 7 indicates that the estimator presented in this paper is superior to the two estimators presented in [24, 27]. The ED estimator with normalized threshold in [24] and the GML estimator in [27] have comparable accuracy and the performances of both of them degrade rapidly as SCR decreases. On the contrary, the accuracy of the estimator proposed in this paper remains constant as the SCR varies.

6. Conclusion

A novel NDA LS TOA estimator is proposed as a solution to overcome the undesired clutter signal for TOA estimation problem in UWB backscattering RFID system. Both theoretical study and simulation results indicate that the estimator is inherently immune to the clutter signal regardless of SNR variation. Simulation results also show that the performance of the estimator depends on the number of sampled symbols as well as the presumed channel delay spread setting. Also the study shows that the estimator is robust over undersampling operation.

Appendices

A.

To prove (18), using conditions $a_m = a_{m+N_a}$ and $N_s = QN_a$, it can be shown that

$$\begin{aligned} A_x(u,v) &= \sum_{m=0}^{N_s-1}\sum_{n=0}^{N_f-1} a_{m-v+\lfloor (n-u)/N_f\rfloor} c_{|n-u|_{N_f}} \\ &= Q\sum_{n=0}^{N_f-1}\left(c_{|n-u|_{N_f}}\varphi\right), \end{aligned} \tag{A.1}$$

where $\varphi = \sum_{m=0}^{N_a-1} a_{m-v+\lfloor (n-u)/N_f\rfloor}$. Letting $i = m - v + \lfloor (n-u)/N_f\rfloor$ and using $a_m = a_{m+N_a}$ again, it is straightforward to show that $\varphi = \sum_{i=0}^{N_a-1} a_i$. Substituting $\varphi = \sum_{i=0}^{N_a-1} a_i$ into (A.1) yields $A_x(u,v) = Q\bar{\omega}(\sum_{i=0}^{N_a-1} a_i)$, where $\bar{\omega} = \sum_{n=0}^{N_f-1}(c_{|n-u|_{N_f}})$. Denoting $j = |n-u|_{N_f}$ and noting that $|-x|_{N_f} = N_f - x$ for $0 < x < N_f - 1$, it is straightforward to derive that $\bar{\omega} = \sum_{j=0}^{N_f-1} c_j$ with which $A_x(u,v)$ becomes

$$A_x(u,v) = Q\left(\sum_{j=0}^{N_f-1} c_j\right)\left(\sum_{i=0}^{N_a-1} a_i\right). \tag{A.2}$$

Analogous to the proof for $A_x(u,v)$, we can also show that $A_y(u,v) = Q(\sum_{j=0}^{N_f-1} c_j)(\sum_{i=0}^{N_a-1} a_i)$. Therefore, we can make the denotation $A_x(u,v) = A_y(u,v) \triangleq A$ where A is a constant.

To prove (22), letting $\Im = \{n = 0, 1, \ldots, N_{f-1},\} \cap \{n \neq u-1\}$, (21) may be rewritten as

$$\begin{aligned} F(u,v) &= Q\sum_{n\in\Im} c_{|n-u|_{N_f}} c_{|n+1-u|_{N_f}} \\ &\quad\times\left(\sum_{m=0}^{N_a-1} a_{m-v+\lfloor (n-u)/N_f\rfloor} a_{m-v+\lfloor (n+1-u)/N_f\rfloor}\right) \\ &\quad + Q\left(\sum_{m=0}^{N_a-1} a_{m-v-1}a_{m-v}\right)\left(c_{N_f-1}c_0\right). \end{aligned} \tag{A.3}$$

Noting that for $n \neq u-1$, we have $|n+1-u|_{N_f} = 1 + |n-u|_{N_f}$ and $m-v+\lfloor (n-u)/N_f\rfloor = m-v+\lfloor (n+1-u)/N_f\rfloor$. Therefore, (A.3) may be rewritten as

$$\begin{aligned} F(u,v) &= QN_a\sum_{n\in\Im} c_{|n-u|_{N_f}} c_{|n-u|_{N_f}+1} \\ &\quad + Q\left(\sum_{m=0}^{N_a-1} a_{m-v-1}a_{m-v}\right)\left(c_{N_f-1}c_0\right). \end{aligned} \tag{A.4}$$

Finally, denoting F as a constant and letting $j = |n-u|_{N_f}$, $i = m - v - 1$, (A.4) becomes

$$F(u,v) = QN_a\sum_{j=0}^{N_f-2} c_j c_{j+1} + Q\left(\sum_{i=0}^{N_a-1} a_i a_{i+1}\right)\left(c_{N_f-1}c_0\right) \triangleq F. \tag{A.5}$$

B.

Using (22) and noting that $C_{m,n}^2(\tilde{u},\tilde{v}) = C_{m,n+1}^2(\tilde{u},\tilde{v}) = 1$, it can be shown that

$$F - N_sN_f = 0 \Longleftrightarrow \frac{1}{2}\sum_m\sum_n\left(C_{m,n}(\tilde{u},\tilde{v}) - C_{m,n+1}(\tilde{u},\tilde{v})\right)^2 = 0. \tag{B.1}$$

Equation (B.1) implies that only when $C_{m,n}(\tilde{u},\tilde{v}) = C_{m,n+1}(\tilde{u},\tilde{v})$, for all m, n, the first equation (29) holds.

With (17) and (22), (B.1) may be derived as

$$\begin{aligned} &\left(F + N_sN_f\right) - \frac{2A^2}{N_sN_f} \\ &\quad= \frac{1}{2}\sum_m\sum_n\left(C_{m,n}(\tilde{u},\tilde{v}) + C_{m,n+1}(\tilde{u},\tilde{v})\right)^2 \\ &\qquad - \frac{\left(A_x + A_y\right)^2}{2N_sN_f} = 0 \\ &\quad\Longleftrightarrow N_sN_f\sum_m\sum_n\left(C_{m,n}(\tilde{u},\tilde{v}) + C_{m,n+1}(\tilde{u},\tilde{v})\right)^2 \\ &\qquad = \left(\sum_m\sum_n\left(C_{m,n}(\tilde{u},\tilde{v}) + C_{m,n+1}(\tilde{u},\tilde{v})\right)\right)^2. \end{aligned} \tag{B.2}$$

To get more insight into the second equation, we invoke the Cauchy-Schwarz inequality which states that $|\sum_i x_i y_i|^2 \leq (\sum_i |x_i|^2)(\sum_i |y_i|^2)$ is always true and the equality holds if and only if $x_i/y_i = x_i/y_i$ for all i, j [37]. Applying the inequality to the right side of (B.2) yields

$$\begin{aligned} &\left(\sum_m\sum_n\left(C_{m,n}(\tilde{u},\tilde{v}) + C_{m,n+1}(\tilde{u},\tilde{v})\right)\right)^2 \\ &\qquad \leq N_sN_f\left(\sum_m\sum_n\left(C_{m,n}(\tilde{u},\tilde{v}) + C_{m,n+1}(\tilde{u},\tilde{v})\right)^2\right), \end{aligned} \tag{B.3}$$

and the equality holds if $C_{m,n}(\tilde{u},\tilde{v}) + C_{m,n+1}(\tilde{u},\tilde{v}) = G$, for all m, n and $G = \pm 2, \text{or}, 0$ is a constant. Note that $G = \pm 2$

is equivalent to $C_{m,n}(\tilde{u},\tilde{v}) = C_{m,n+1}(\tilde{u},\tilde{v})$ since $C_{m,n}(\tilde{u},\tilde{v})$ and $C_{m,n+1}(\tilde{u},\tilde{v})$ can only be $+1$ or -1. In conclusion, when $C_{m,n}(\tilde{u},\tilde{v}) = C_{m,n+1}(\tilde{u},\tilde{v})$, for all m,n or $C_{m,n}(\tilde{u},\tilde{v}) + C_{m,n+1}(\tilde{u},\tilde{v}) = 0$, for all m,n are fulfilled, at least one of (29) and (30) holds and the expression (27) becomes invalid.

Acknowledgment

This paper was supported by the ASTAR SERC Project under Grant no. 052-121-0086.

References

[1] R. Want, "An introduction to RFID technology," *IEEE Pervasive Computing*, vol. 5, no. 1, pp. 25–33, 2006.

[2] "First report and order in the matter of revision of part 15 of commission's rules regarding ultra-wideband transmission systems," Tech. Rep., FCC, 2002.

[3] M. Z. Win and R. A. Scholtz, "On the robustness of ultra-wide bandwidth signals in dense multipath environments," *IEEE Communications Letters*, vol. 2, no. 2, pp. 51–53, 1998.

[4] R. J. Fontana and S. J. Gunderson, "Ultra-wideband precision asset location system," in *Proceedings of the Ultra Wideband Systems and Technologies (UWBST '02)*, vol. 21, pp. 147–150, Baltimore, Md, USA, May 2002.

[5] S. Gezici, Z. Tian, G. B. Giannakis et al., "Localization via ultra-wideband radios: a look at positioning aspects of future sensor networks," *IEEE Signal Processing Magazine*, vol. 22, no. 4, pp. 70–84, 2005.

[6] D. Dardari, C.-C. Chong, and M. Z. Win, "Threshold-based time-of-arrival estimators in UWB dense multipath channels," *IEEE Transactions on Communications*, vol. 56, no. 8, pp. 1366–1378, 2008.

[7] D. Dardari, C.-C. Chong, and M. Z. Win, "Analysis of threshold-based TOA estimator in UWB channels," in *Proceedings of the European Signal Processing Conference (EUSIPCO '06)*, Florence, Italy, September 2006.

[8] D. Dardari, "Pseudorandom active UWB reflectors for accurate ranging," *IEEE Communications Letters*, vol. 8, no. 10, pp. 608–610, 2004.

[9] D. Dardari and R. D'Errico, "Passive ultrawide bandwidth RFID," in *Proceedings of the IEEE Global Telecommunications Conference (GLOBECOM '08)*, pp. 3947–3952, New Orlean, Lo, USA, December 2008.

[10] S. Hu, C. L. Law, and W. Dou, "Measurements of UWB antennas backscattering characteristics for RFID systems," in *Proceedings of the IEEE International Conference on Ultra-Wideband (ICUWB '07)*, pp. 94–99, Singapore, September 2007.

[11] E. Paolini, A. Giorgetti, M. Chiani, R. Minutolo, and M. Montanari, "Localization capability of cooperative anti-intruder radar systems," *Eurasip Journal on Advances in Signal Processing*, vol. 2008, Article ID 726854, 14 pages, 2008.

[12] V. Lottici, A. D'Andrea, and U. Mengali, "Channel estimation for ultra-wideband communications," *IEEE Journal on Selected Areas in Communications*, vol. 20, no. 9, pp. 1638–1645, 2002.

[13] R. J.-M. Cramer, R. A. Scholtz, and M. Z. Win, "Evaluation of an ultra-wide-band propagation channel," *IEEE Transactions on Antennas and Propagation*, vol. 50, no. 5, pp. 561–570, 2002.

[14] J.-Y. Lee and R. A. Scholtz, "Ranging in a dense multipath environment using an UWB radio link," *IEEE Journal on Selected Areas in Communications*, vol. 20, no. 9, pp. 1677–1683, 2002.

[15] I. Maravic, J. Kusuma, and M. Vetterli, "Low-sampling rate UWB channel characterization and synchronization," *Journal of Communications and Networks*, vol. 5, no. 4, pp. 319–326, 2003.

[16] J. Kusuma, I. Maravic, and M. Vetterli, "Sampling with finite rate of innovation: channel and timing estimation for UWB and GPS," in *Proceedings of the International Conference on Communications (ICC '03)*, vol. 5, pp. 3540–3544, Anchorage, AK, USA, May 2003.

[17] X. Li and K. Pahlavan, "Super-resolution TOA estimation with diversity for indoor geolocation," *IEEE Transactions on Wireless Communications*, vol. 3, no. 1, pp. 224–234, 2004.

[18] C. Falsi, D. Dardari, L. Mucchi, and M. Z. Win, "Time of arrival estimation for UWB localizers in realistic environments," *Eurasip Journal on Applied Signal Processing*, vol. 2006, Article ID 32082, 13 pages, 2006.

[19] S. H. Song and Q. T. Zhang, "Multi-dimensional detector for UWB ranging systems in dense multipath environments," *IEEE Transactions on Wireless Communications*, vol. 7, no. 1, pp. 175–183, 2008.

[20] L. Yang, Z. Tian, and G. B. Giannakis, "Non-data aided timing acquisition of ultra-wideband transmissions using cyclostationarity," in *Proceedings of the IEEE International Conference on Accoustics, Speech, and Signal Processing*, pp. 121–124, Hong Kong, April 2003.

[21] Z. Tian, L. Yang, and G. B. Giannakis, "Symbol timing estimation in ultra wideband communications," in *Proceedings of the 36th Asilomar Conference on Signals Systems and Computers*, pp. 1924–1928, Pacific Grove, Calif, USA, November 2002.

[22] L. Yang and G. B. Giannakis, "Timing ultra-wideband signals with dirty templates," *IEEE Transactions on Communications*, vol. 53, no. 11, pp. 1952–1963, 2005.

[23] Z. Tian and G. B. Giannakis, "A GLRT approach to data-aided timing acquisition in UWB radios—part I: algorithms," *IEEE Transactions on Wireless Communications*, vol. 4, no. 6, pp. 2956–2967, 2005.

[24] I. Guvenc and Z. Sahinoglu, "Threshold-based TOA estimation for impulse radio UWB systems," in *Proceedings of the IEEE International Conference on Ultra-Wideband (ICUWB '05)*, vol. 2005, pp. 420–425, Zurich, Switzerland, 2005.

[25] I. Guvenc and Z. Sahinoglu, "Threshold selection for UWB TOA estimation based on kurtosis analysis," *IEEE Communications Letters*, vol. 9, no. 12, pp. 1025–1027, 2005.

[26] C. Xu and C. L. Law, "Delay-dependent threshold selection for UWB TOA estimation," *IEEE Communications Letters*, vol. 12, no. 5, pp. 380–382, 2008.

[27] A. Rabbachin, I. Oppermann, and B. Denis, "GML ToA estimation based on low complexity UWB energy detection," in *Proceedings of the IEEE 17th International Symposium on Personal, Indoor and Mobile Radio Communications (PIMRC '06)*, pp. 1–5, Helsinki, Finland, September 2006.

[28] C. Carbonelli and U. Mengali, "Synchronization algorithms for UWB signals," *IEEE Transactions on Communications*, vol. 54, no. 2, pp. 329–338, 2006.

[29] A. A. D'Amico, U. Mengali, and L. Taponecco, "Energy-based TOA estimation," *IEEE Transactions on Wireless Communications*, vol. 7, no. 3, pp. 838–847, 2008.

[30] S. Gezici, Z. Sahinoglu, A. F. Molisch, H. Kobayashi, and H. V. Poor, "Two-step time of arrival estimation for pulse-based ultra-wideband systems," *Eurasip Journal on Advances in Signal Processing*, vol. 2008, Article ID 529134, 11 pages, 2008.

[31] J. Ibrahim and R. M. Buehrer, "Two-stage acquisition for UWB in dense multipath," *IEEE Journal on Selected Areas in Communications*, vol. 24, no. 4 I, pp. 801–807, 2006.

[32] D. Dardari, A. Conti, U. Ferner, A. Giorgetti, and M. Z. Win, "Ranging with ultrawide bandwidth signals in multipath environments," *Proceedings of the IEEE*, vol. 97, no. 2, pp. 404–425, 2009.

[33] S. Hu, H. Chen, et al., "Backscattering cross section of ultra-wideband antennas," *IEEE Antennas and Wireless Propagation Letters*, vol. 6, pp. 70–73, 2007.

[34] S. Boyd and L. Vandenberghe, *Convex Optimization*, Cambridge University Press, New York, NY, USA, 2004.

[35] J. F. Bonnans, et al., *Numerical Optimization—Theoretical and Practical Aspects*, Springer, New York, NY, USA, 2006, Section Edition.

[36] A. F. Molisch, et al., "IEEE 802.15.4a channel model—final report," Document IEEE 802.15-04-0662-02-004a, 2005.

[37] M. Abramowitz and I. A. Stegun, *Handbook of Mathematical Function with Formulas, Graphs, and Mathematical Tables*, Dover, New York, NY, USA, 1970.